NANO LETTERS

Letter

pubs.acs.org/NanoLett

Role of the Seeding Promoter in MoS_2 Growth by Chemical Vapor Deposition

Xi Ling,[†] Yi-Hsien Lee,*[,‡] Yuxuan Lin,[†] Wenjing Fang,[†] Lili Yu,[†] Mildred S. Dresselhaus,[†,§] and Jing Kong*[,†]

[†]Department of Electrical Engineering and Computer Sciences, Massachusetts Institute of Technology, Cambridge, Massachusetts 02139, United States

[‡]Material Sciences and Engineering, National Tsing-Hua University, Hsinchu, 30013, Taiwan

[§]Department of Physics, Massachusetts Institute of Technology, Cambridge, Massachusetts 02139, United States

Supporting Information

ABSTRACT: The thinnest semiconductor, molybdenum disulfide (MoS_2) monolayer, exhibits promising prospects in the applications of optoelectronics and valleytronics. A uniform and highly crystalline MoS_2 monolayer in a large area is highly desirable for both fundamental studies and substantial applications. Here, utilizing various aromatic molecules as seeding promoters, a large-area, highly crystalline, and uniform MoS_2 monolayer was achieved with chemical vapor deposition (CVD) at a relatively low growth temperature (650 °C). The dependence of the growth results on the seed concentration and on the use of different seeding promoters is further investigated. It is also found that an optimized concentration of seed molecules is helpful for the nucleation of the MoS_2. The newly identified seed molecules can be easily deposited on various substrates and allows the direct growth of monolayer MoS_2 on Au, hexagonal boron nitride (h-BN), and graphene to achieve various hybrid structures.

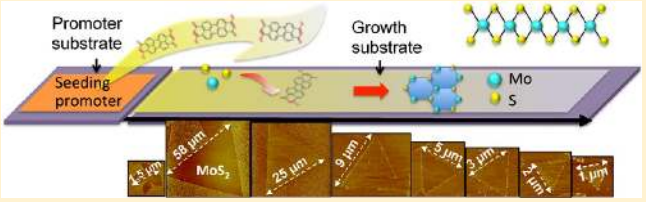

KEYWORDS: *Transition metal dichalcogenides, seed, $F_{16}CuPc$, heterogeneous nucleation, hybrid structure*

In recent years, two-dimensional monolayers of layered materials, including graphene, hexagonal boron nitride (h-BN), and transition metal dichalcogenides (TMDs), have attracted much attention due to their unique structures and remarkable properties.[1−9] As a member of the TMD family, molybdenum disulfide (MoS_2) with a direct bandgap is complementary to the gapless graphene and suggests a great potential for logic devices, integrated circuits, and optoelectronics. Thus, it is highly desirable to develop reliable and scalable synthesis methods for MoS_2. The growth of graphene and insulating h-BN have been extensively studied with chemical vapor deposition (CVD) method.[10−14] However, the CVD of MoS_2 has only been reported since last year.[15,16] Several different precursors have been used to synthesize MoS_2 using CVD, such as $(NH_4)_2MoS_4$,[17,18] Mo film,[16] MoO_3,[15,19−23] and $MoCl_4$.[24] Recently, Wu et al.[25] reported the vapor−solid growth of MoS_2 monolayer under the low pressure by directly using MoS_2 powder as a source. Among them, approaches using solid state precursors of MoO_3 and sulfur powder have become dominant due to the relative simplicity and the preference of MoS_2 monolayer growth. At elevated temperatures, the sulfur vapor is introduced with an inert carrier gas to react with the MoO_x (from MoO_3) for MoS_2 monolayer growth on a substrate by the sulfurization reaction.[26] Most reported MoS_2 monolayer growth were carried out on the blank SiO_2/Si substrate.[21,22] However, Lee et al.[15] reported a synthetic process for high quality monolayer MoS_2 by loading either perylene-3,4,9,10-tetracarboxylic acid tetrapotassium salt (PTAS), 3,4,9,10-perylene-tetracarboxylicacid-dianhydride (PTCDA), or reduced graphene oxide (r-GO) as seeding promoters on the SiO_2/Si substrate. In this work, further investigation on the role of the seeding promoter in synthesizing MoS_2 monolayers was systematically studied. By examining the growth results at different distances away from the source of the seeding promoters, we demonstrate the importance of the promoters with proper concentration in facilitating the nucleation of MoS_2 monolayer on the growth substrate. Moreover, in addition to the already identified seeding promoters,[15,19] various other aromatic molecules were further investigated, and many of them were found to be effective as seeding promoters for the growth of MoS_2. In contrast, no enhancement in monolayer MoS_2 growth was observed when inorganic nanoparticles were used. These newly identified seeding molecules can be uniformly deposited on diverse substrates by thermal evaporation (in contrast, the previous seeding promoters were deposited via aqueous solution[15,19]), thus facilitating the direct growth of MoS_2 on diverse hydrophobic substrates, such as gold, graphene, and h-

Received: September 9, 2013
Revised: January 9, 2014
Published: January 29, 2014

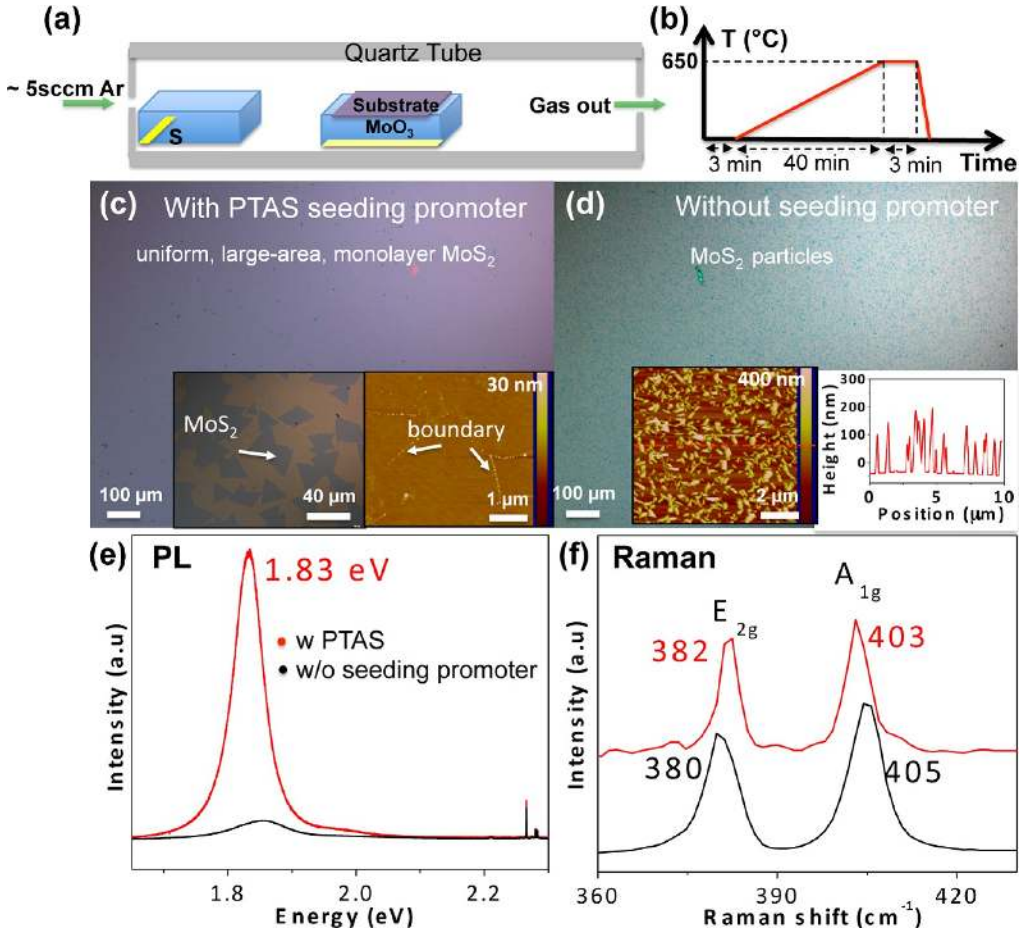

Figure 1. (a) A schematic illustration of the MoS_2 CVD system. (b) The temperature programming process used for a typical growth. (c–d) Typical growth results obtained with (c) and without (d) using PTAS as a seeding promoter. The insets in (c) are the optical image of the triangular MoS_2 flakes at the edge of the MoS_2 monolayer film, and the AFM image on the continuous MoS_2 monolayer film. The insets in (d) are the AFM image of the MoS_2 particles deposited on the surface and the corresponding height cross-section analysis. (e–f) Typical PL (e) and Raman (f) spectra of MoS_2 samples that were prepared with (red) and without (black) PTAS seeding promoter. The PL intensities are normalized by the intensities of the A_{1g} Raman mode. The excitation wavelength is 532.5 nm.

BN. This advancement significantly enables the growth of hybrid structures among functional materials, TMD monolayers, and graphene-like two-dimensional materials.[27−30]

Figure 1a–b shows an illustration of the CVD setup for MoS_2 growth and typical growth conditions. Briefly, 0.018 g of MoO_3 (molybdenum oxide) powder in a ceramic crucible was placed in the center of the furnace. Also 0.016 g of sulfur powder was placed in a crucible 15 cm away from the center of a quartz tube. The substrate was placed face-down on the crucible of the MoO_3 powder. Some 5 sccm Ar was used as a carrying gas. The growth temperature was controlled at 650 °C (Figure 1b). A continuous, large-area MoS_2 monolayer can be typically achieved using PTAS as seeding promoters (Figure 1c). The atomic force microscopy (AFM) image (Figure 1c, right inset) displays that the as-grown MoS_2 monolayer is flat and clean. Some boundaries are visible due to the merging of the triangular domains. At the edge regions of a continuous film, isolated triangular MoS_2 domains with lateral sizes around 50 μm can be seen (Figure 1c, left inset). In contrast, only MoS_2 particles were grown on the substrate without using the seeding promoters (Figure 1d). These MoS_2 particles have thicknesses between 1 and 200 nm, as can be seen from the AFM images in the inset of Figure 1d. These MoS_2 monolayer and particles were further characterized by photoluminescence (PL) and Raman spectroscopy (Figure 1e–f). The monolayer MoS_2 grown with the PTAS seed exhibits an intense PL at around 1.83 eV with a fwhm (full width at half-maximum intensity) of about 55 meV, which is consistent with a direct bandgap of the monolayer MoS_2 (Figure 1e).[21] The strong PL intensity and small PL width suggest a high quality for the MoS_2 monolayer.[21,31] In contrast, a weak PL intensity of the MoS_2 particles in the low temperature synthesis without using any seed is identified as being due to the low luminescence quantum efficiency of the multilayer MoS_2.[31] In addition, the frequency difference between the E_{2g} and A_{1g} Raman modes depends on the number of layers of the MoS_2 sample, which is about 20 cm^{-1} for monolayer MoS_2 and about 25 cm^{-1} for bulk MoS_2.[32,33] Here, the fitting results show that these two modes are located at 382 and 403 cm^{-1} for the MoS_2 monolayer, where the frequency difference is about 21 cm^{-1}, while they are at 380 and 405 cm^{-1} with a frequency difference of 25 cm^{-1} for the MoS_2 particles (Figure 1f). These results further indicate that by using PTAS seeding promoter, MoS_2 monolayer growth can be obtained easily, while without using the seeding promoter, random MoS_2 particle growth is preferred under the growth conditions used by this work. These comparative results suggest that the PTAS seeding promoter must play an important role in facilitating the monolayer MoS_2 growth here.

dx.doi.org/10.1021/nl4033704 | Nano Lett. 2014, 14, 464−472

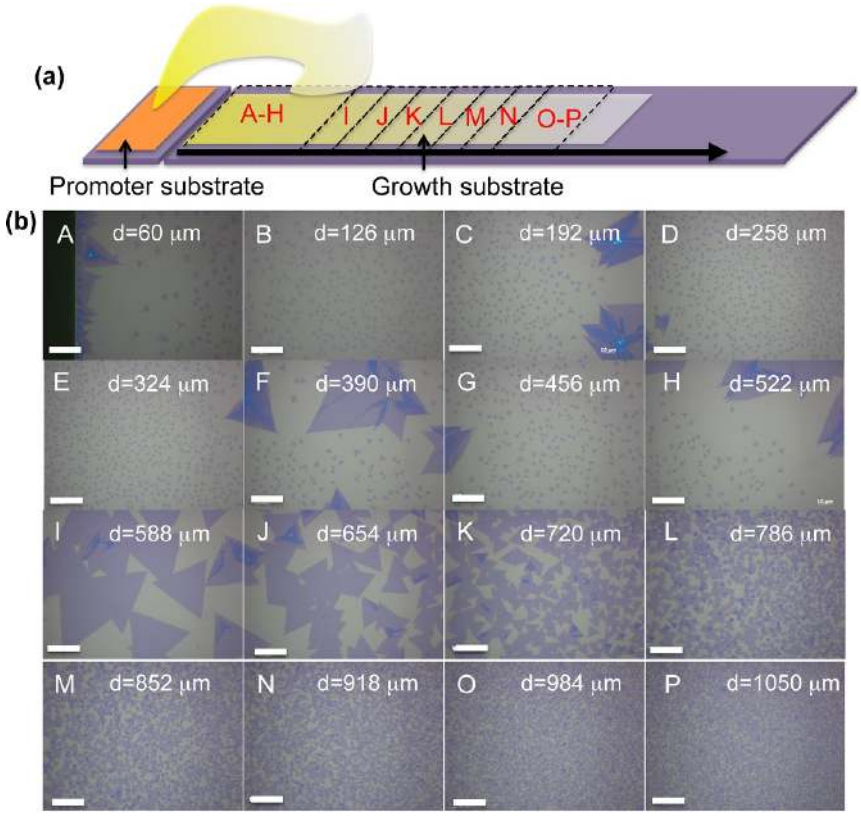

Figure 2. (a) A schematic illustration of the promoter substrate and the growth substrate as well as the various divisions (A–P) according to the distance *d* away from the promoter substrate on the growth substrate. (b) The corresponding optical images of the MoS_2 flakes in different regions of the growth substrate. Scale bars: 20 μm.

To further study how the concentration of the seeding molecule influences the growth result, a promoter substrate covered with condensed PTAS seeding promoters (2–3 μL of PTAS solution was dropped on the surface and left to dry naturally) was placed upstream of a growth substrate (Figure 2a). This study was carried out because very often in our experiments it was observed that, even when seeding molecules were patterned in a certain region on the substrate, MoS_2 monolayers also grew in the regions away from the seeding pattern, suggesting the diffusion of the seeding molecules (or fragments of the seeding molecule) at elevated temperature during the growth. Therefore a study as shown in Figure 2a should give better understanding for this aspect. It is anticipated that such diffusion should result in a concentration gradient away from the promoter region over the growth substrate (the detailed growth setup is shown in part 1 of the Supporting Information (SI)). The concentration of the seeding promoter is anticipated to decrease with the distance away from the promoter substrate (Figure 2a). The growth substrate is divided into several regions from A to P each having about a 60–70 μm width. The growth results in each region (with d labeled as the distance between the center of its image and the edge of the promoter substrate) are shown by the optical images (Figure 2b). It can be seen that, although there is no seeding molecule deposited on the growth substrate, monolayer flakes are observed in most of these regions, similar to the results obtained with seeding promoters being applied. Nevertheless, the flake sizes and surface coverage show an interesting variation along *d*: when *d* is less than 600 μm (Figure 2b, regions A–H), the MoS_2 flakes are not exactly triangles with sharp edges as normally observed, but rather a star shape, the flake sizes are around 2–3 μm with more or less similar density across those regions, and occasionally a much larger flake (>60 μm, though most often with few-layer regions) is observed, as can be seen in Figure 2b for regions C, F, and H. For *d* is ~600 μm, large monolayer flakes with sizes ~60 μm are observed. In regions I–P, the monolayer flake sizes decrease as *d* increases further. With a distance 1 mm away from the seeding promoter source (Figure 2b, region P), the flake size becomes ~1 μm again, but the flake density appears to be much larger than in regions A–H.

The growth results in these regions were further examined using AFM, PL, and Raman characterization (Figure 3). For regions A–H, although the monolayer triangular MoS_2 flake density appears to be low, AFM characterization reveals a large density of MoS_2 particles with ~50 nm size and 4–5 nm in thickness over the whole background. The AFM images of these regions, as well as the PL and Raman characterization of the background are shown in Figure S2 of the SI, revealing that the small particles in the background are MoS_2 flakes. Even with such a rough background (roughness Ra = ~0.6 nm), the monolayer MoS_2 flakes are very flat (Ra = ~0.2 nm) and clean on the surface. The roughness of the background decreases with the increase of the distance away from the promoter substrate (Table S1). This indicates a decrease of the nucleation sites with decreasing seeding promoter concentration. The same background persists even in regions I and J, where large flakes of monolayer MoS_2 are grown. In contrast, the regions further away (N to P) have a cleaner background and show a decreasing flake sizes together with increasingly higher flake densities. The MoS_2 coverage extracted from the optical images in these regions is about similar (~60%), which

dx.doi.org/10.1021/nl4033704 | *Nano Lett.* 2014, 14, 464–472

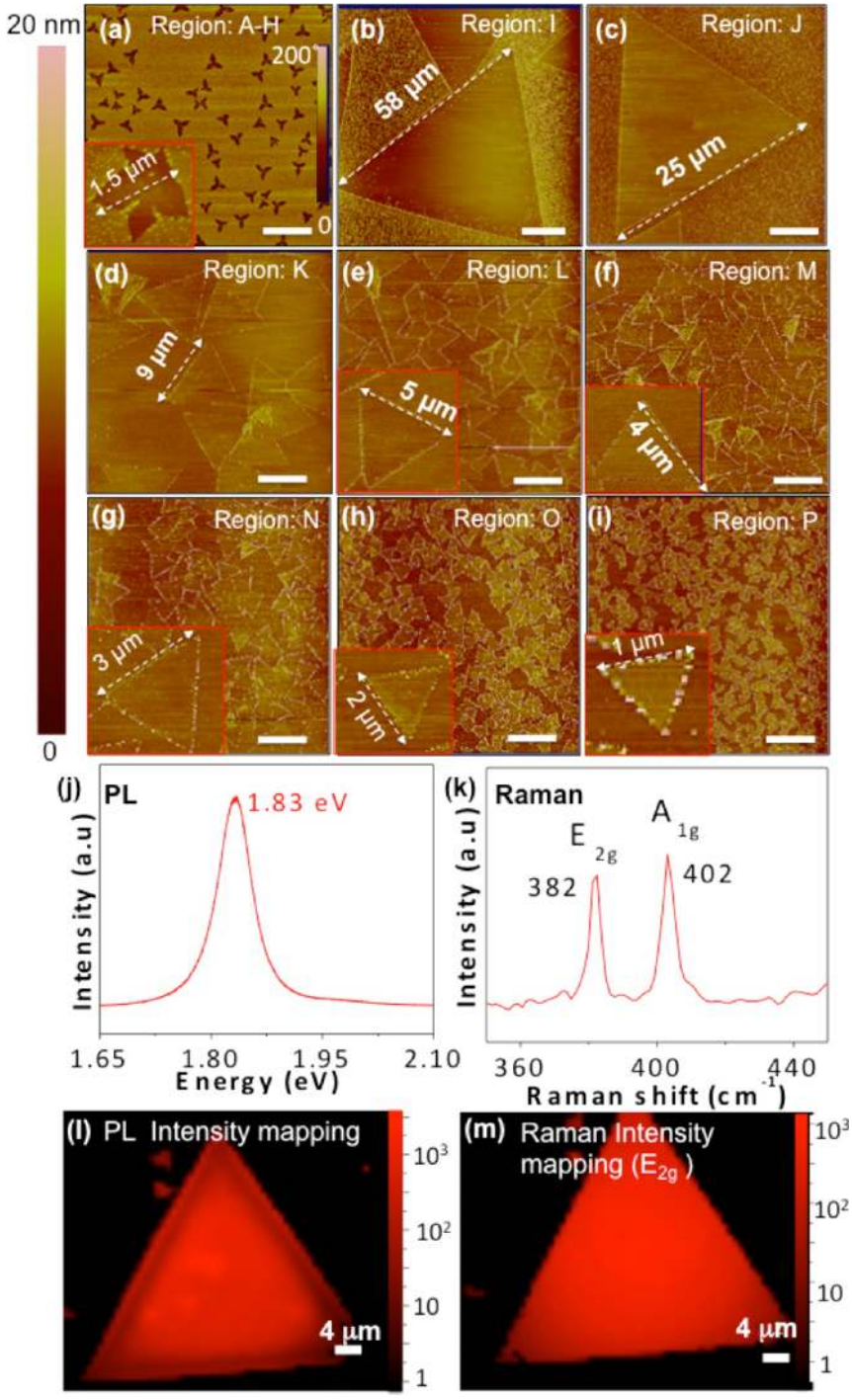

Figure 3. (a–i) AFM height images (except (a) which is the phase image) of MoS_2 domains on different regions of the growth substrate. The insets show the corresponding zoom in images. The domain sizes are marked on each of the images. Scale bar: 5 μm (except 10 μm in b). (j–k) Typical PL (j) and Raman (k) spectra of the triangular MoS_2 domains. (l–m) The mapping images of the intensity of PL (l) and E_{2g} Raman mode (m) of a triangular MoS_2 flake in the region J. The excitation wavelength is 532.5 nm.

is consistent with the fact that reduced flake sizes are compensated by the higher flake densities. The optical properties of the as-grown MoS_2 flakes were studied by Raman and PL spectroscopy, as shown in Figure 3j–k. A strong PL signal is located at 1.83 eV, and the frequency difference between the Raman modes E_{2g} (382 cm^{-1}) and A_{1g} (402 cm^{-1}) is 20 cm^1, indicating a high crystallinity of the as-grown MoS_2 monolayer. The mapping images of the intensity of the PL and the E_{2g} mode are shown in Figure 3l–m, suggesting a high crystallinity and uniformity of the MoS_2 monolayer. More mapping results regarding other spectral parameters are shown in part 3 of the SI.

The observation of distance-dependent growth suggests that there is an optimum seeding promoter concentration for growing MoS_2 with a large domain size. A higher seeding promoter concentration may result in higher density of nucleation sites and smaller domains (corresponding to regions A–H). This is further supported by the observation of the

dx.doi.org/10.1021/nl4033704 | Nano Lett. 2014, 14, 464–472

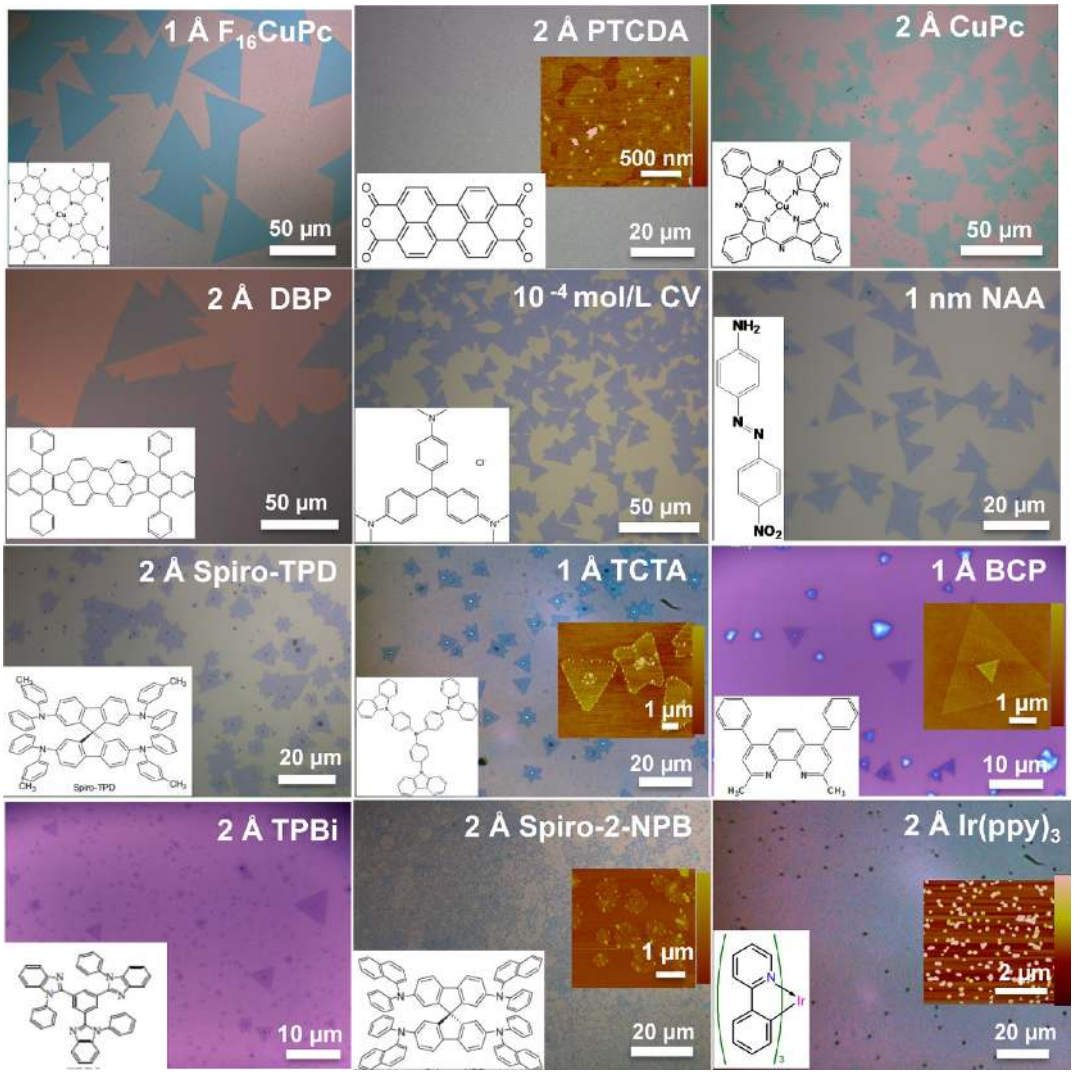

Figure 4. Typical optical images of the surface after the MoS_2 growth using different aromatic molecules as seeding promoters. The names and thicknesses of the seeding promoters are labeled on the images. The insets show the corresponding molecular structures or AFM images of the surface after MoS_2 growth. The color bars in the AFM images are 10 nm for PTCDA, 20 nm for TCTA and Spiro-2-NPB, 30 nm for BCP, and 50 nm for $Ir(ppy)_3$.

result on the promoter substrate where the domain size is small and multilayer MoS_2 flakes prefers to grow (see part 4 of the SI). Regions A−H are closer to the promoter substrate, and it is anticipated that the concentration of the PTAS seeding promoter is high, which likely leads to the formation of a large amount of nucleation sites as a rough background.

The comparisons carried out in Figures 1−3 also suggest that the PTAS seeding promoter influences whether the growth mode is layered growth or island growth. The mechanism of thin film growth depends on the surface energy and chemical potentials of the deposited layers and their substrates.[34,35] When the surface adhesive force is stronger than the adatom cohesive force, layer growth is preferred. Otherwise, island growth dominates. Here, the presence of PTAS possibly increases the surface adhesive force of MoS_2, which results in the layered growth of MoS_2. Furthermore, PTAS may offer a heterogeneous nucleation site for the formation of MoS_2 nuclei, which need less energy than that for homogeneous nucleation. In this aspect, its role will be similar to the role played by the patterned graphene islands in ref 35. Nevertheless, as currently these molecules cannot be identified in the lattice due to their small size, further in-depth studies are needed. The promotion of the heterogeneous nucleation process is mainly attributed to the lower surface energy due to the wetting, which will diminish the free energy barrier and facilitate the nucleation.[36−38] The free energy needed for the heterogeneous nucleation can be expressed as $\Delta G_{Hetero} = \Delta G_{Homo} f(\theta)$, where $f(\theta) = 1/2 - 3/4 \cos\theta + 1/4 \cos^3\theta$, and ΔG_{Homo} is the free energy needed for the homogeneous nucleation while θ is the contact angle between the nucleation site and the material being grown.[36] When $\theta = 180°$, $f(\theta) = 1$. Then, there is no wetting of the surface, which results in falling into the case of homogeneous nucleation. However, when $\theta = 0°$, $f(\theta) = 0$. It indicates the full wetting, which results in no barrier for nucleation at surface. This possibly is also the reason why we can grow MoS_2 at lower temperature in the presence of the PTAS seeding promoter. Based on these results, we expect there should be other molecular seeding promoters that can facilitate the nucleation of MoS_2 by lowering the free energy for the nucleation, as well as can benefit layer growth by increasing the surface adhesive energy.

dx.doi.org/10.1021/nl4033704 | Nano Lett. 2014, 14, 464−472

Table 1. Summary of the Growth Results Using Different Kinds of Seeding Promoters

			growth results		
types	seeding promoter	sublimation/decomposition temperature[a] (°C)[44]	domain size (μm)	thickness[b]	overall quality
organic	PTAS	>600 (s)[c]/high (d)	~60	1L	excellent
	F_{16}CuPc	>430 (s)	~60	1L	excellent
	PTCDA	>450 (s)	continuous film	1L	good
	CuPc	>430 (s)	~30	1L	good
	DBP	350–450 (s)	~50	1L	good
	CV	~205 (d)[43]	~20	1L	good
	NAA	~200 (d)[45]	~15	1L	good
	spiro-TPD	>280 (s)	~10	1L	fair
	TCTA	>410 (s)	~10	1L and ML	fair
	BCP	>240 (s)/300 (d)	~5	1L and ML	fair
	TPBI	>350 (s)	~5	1L and ML	poor
	spiro-2-NPB	>390 (s)	~1	1L and ML	poor
	$Ir(ppy)_3$	>300 (s)	N/A	ML	bad
inorganic	Al_2O_3	high (s&d)	N/A	almost nothing	bad
	HfO_2	high (s&d)	N/A	almost nothing	bad
	5 Å Au	high (s&d)	N/A	particles	bad
	bare Si	high (s&d)	N/A	almost nothing	bad

[a]The sublimation temperature is from thermogravimetry analysis (TGA). [b]1L: monolayer; ML: multilayer. [c]s: sublimation; d: decomposition.

Here, we further make an attempt to use other organic molecules or inorganic particles to grow MoS_2. Twelve kinds of aromatic molecules, including copper(II) 1,2,3,4,8,9,10,11,15,16,17,18,22,23,24,25-hexadecafluoro-29*H*,31*H*-phthalocyanine (F_{16}CuPc), PTCDA, copper phthalocyanine (CuPc), dibenzo{[*f*,*f*′]-4,4′,7,7′-tetraphenyl-diindeno[1,2,3-*cd*:1′,2′,3′-*lm*]perylene (DBP), 4′-nitrobenzene-diazoaminoazobenzene (NAA), *N*,*N*′-bis(3-methylphenyl)-*N*,*N*′-diphenyl-9,9-spirobifluorene-2,7-diamine (spiro-TDP), tris(4-carbazoyl-9-ylphenyl) amine (TCTA), bathocuproine (BCP), 1,3,5-tris(*N*-phenylbenzimiazole-2-yl)benzene (TPBi), 2,2′,7,7′-tetra(*N*-phenyl-1-naphthyl-amine)-9,9′-spirobifluorene (spiro-2-NPB), and iridium, tris(2-phenylpyidine) ($Ir(ppy)_3$), as well as four kinds of inorganic particles, including Al_2O_3 (aluminum oxide), HfO_2 (hafnium oxide), bare Si (with a very thin SiO_2 layer by natural oxidation), and Au, were used as seeding promoters to grow MoS_2. Figure 4 shows the typical optical images of the surface after MoS_2 growth for all of the organic seeding promoters (AFM images are given for some of them as some have small domains and are hard to see under optical imaging). The growth results for the inorganic particles are shown in part 5 of the SI. For most of the organic molecules (except $Ir(ppy)_3$ and spiro-2-NPB), a continuous monolayer film or triangular flakes are observed on the substrates after the growth. However, for the inorganic seeding promoters, either no MoS_2 growth was obtained (in the case of Al_2O_3, HfO_2, and bare Si) or only MoS_2 particles (in the case of Au, similar to the case of without seeding promoter in Figure 1d). The PL and Raman results indicate that the growth yields monolayer MoS_2 for most of the aromatic seeding promoters (except for $Ir(ppy)_3$, in which case multilayer MoS_2 or particles were grown) (Figures S6 and S7 and Table S2 in part 6 of the SI). It should be mentioned that the growth condition (MoO_3 and S amount, temperature, the distance between the crucibles, gas flow rate, etc.) for these seeding promoters were not yet optimized, but rather, the same growth condition as that tuned for the PTAS seeding promoter was also used for all 12 cases listed above. Nevertheless, the results obtained here can already provide a qualitative evaluation of the potential of these potential seeding promoters.

From these studies, we found that, under the current growth conditions, F_{16}CuPc is a seeding promoter comparable in performance to PTAS, which can facilitate the growth of large-area, high-quality, and uniform monolayer MoS_2 growth (more characterizations are shown in part 7 of the SI). For other molecules under the current growth condition, the resulting MoS_2 flake sizes that were obtained follow the order: (CuPc, PTCDA, DBP, CV) > (NAA, spiro-TDP, TCTA) > (BCP, TPBi, spiro-2-NPB, $Ir(ppy)_3$). However, for the inorganic seeding promoters, no monolayer MoS_2 was formed during their growth processes. When using the 5 Å Au as seeding promoter, only MoS_2 particles were obtained by the island growth mechanism. It should be mentioned that, besides the aromatic structure of the seeding molecules, the sublimation temperature and the decomposition temperature also need to be considered as a requirement for a promising seeding promoters, since the growth is carried out at high (650 °C) temperature. In Table 1, we summarize the feature of the seeding promoters, as well as the corresponding growth results. Among the organic seeding promoters, F_{16}CuPc has the highest stability at high temperature,[39] which might be a favorable factor for promoting the growth. On the other hand, some of seeding promoters sublimate at relatively low temperatures and are very easy to decompose, such as BCP, TPBi, spiro-2-NPB, and $Ir(ppy)_3$, which might be one reason for their limited capability in promoting MoS_2 growth.

Identifying the new seeding molecules also greatly facilitates the fabrication of hybrid structures involving MoS_2. Hybrid structures among TMD monolayers, graphene-like 2D materials, and some other functional materials, such as graphene, h-BN, and metals, exhibits fascinating properties for applications in high-performance electronic and optoelectronic devices.[28,30,40−43] PTAS as a seeding promoter works exceedingly well for promoting MoS_2 growth on hydrophilic substrates, since it is a salt and is typically applied with an aqueous solution. However, applying PTAS uniformly on hydrophobic substrates becomes challenging. Thus, for future applications, we could deposit F_{16}CuPc seeding promoter via thermal evaporation on these substrates. These seeding promoters and the PTAS are complementary to each other.

dx.doi.org/10.1021/nl4033704 | *Nano Lett.* 2014, 14, 464−472

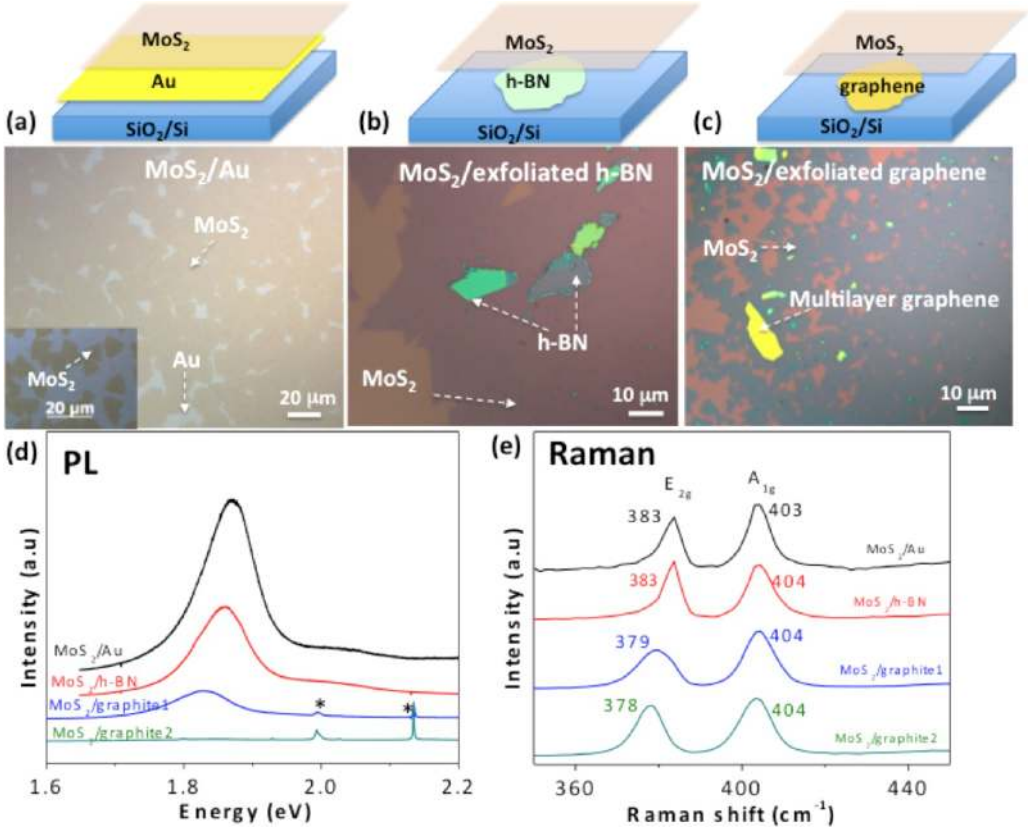

Figure 5. (a–c) Typical OM images of the hybrid structures by using $F_{16}CuPc$ as a seeding promter: (a) MoS_2/Au/SiO_2/Si; (b) MoS_2/exfoliated h-BN/SiO_2/Si; (c) MoS_2/ exfoliated graphene/SiO_2/Si. The schematic illustrations of the corresponding hybrid structures are shown above the optical images. (d–e) The corresponding PL (d) and Raman (e) spectra of MoS_2 on Au, h-BN, and graphene (or graphite). The excitation wavelength is 532.5 nm.

The $F_{16}CuPc$ molecules were confirmed to be on the surface by the Raman spectral characterization. The Raman signals of $F_{16}CuPc$ on graphene can still be observed after annealing the composite sample at 650 °C (the growth temperature) for 1 h (see part 8 of the SI). Here, we shows typical optical images of MoS_2 grown directly on a 100 nm Au/SiO_2/Si substrate and on exfoliated h-BN/SiO_2/Si and exfoliated graphene/SiO_2/Si substrates by evaporating 2 Å $F_{16}CuPc$ on each of the substrates as a seeding promoter (Figure 5a–c). The resulting whole surface of the substrate in this case is covered by a continuous MoS_2 monolayer. This result was not achieved by using PTAS as seeding promoter since PTAS solution is hard to deposit on these kinds of substrates uniformly. The PL and Raman spectra were collected on the area with Au, h-BN, and graphene (graphite) (Figure 5d–e). The PL signal and the E_{2g} and A_{1g} Raman modes indicate MoS_2 is obtained on the Au, h-BN, and graphene (graphite) substrates, even though the contrast differences in the optical images are not strong enough to see if there is MoS_2 on the surface of h-BN or graphite. The MoS_2 films in these structures were confirmed to be of monolayer thickness by TEM study on CVD grown samples (data not shown here). It should be noted that, if there was no $F_{16}CuPc$ seeding promoter on these substrates, no MoS_2 monolayers were obtained on the substrates (see part 9 in the SI). Since there are some specific interaction effects on such hybrid structures, some interesting phenomena were observed, such as the enhancement of the PL intensity on Au and the quenching of the PL intensity on the h-BN and graphene (graphite) substrates, and the shift of the PL and Raman peak frequencies. The detailed studies of these hybrid structures are presently under investigation and will be presented in a future report.

In conclusion, the importance of the seeding molecule in facilitating the growth of MoS_2 was investigated. Comparing the growth result with and without using the PTAS seeding promoter, it is clear that a large-area, continuous, and high-quality MoS_2 monolayer can be obtained under relatively low temperature (650 °C) conditions using PTAS as a seeding promoter, while only MoS_2 particles are obtained using the same growth conditions but without any seeding promoter. Moreover, by using a seeding promoter and examining the growth result on a nearby substrate as a function of distance between the promoter substrate and the growth regions, it is revealed that an optimum seed concentration is essential for the growth of MoS_2 monolayer. In addition to PTAS, 12 organic seeding promoters and four inorganic seeding promoters were examined in the present study for the growth of MoS_2. It is found that, similar to PTAS, some of the aromatic organic molecules can also assist the growth of monolayer MoS_2, while this characteristic has not been found in the inorganic particles investigated in this work. Among the organic ones, $F_{16}CuPc$ is found to be a promising seeding promoter for the growth under the current growth condition, allowing the fabrication of hybrid structures between MoS_2 monolayers, and Au, h-BN and graphene (graphite). It is anticipated that these studies will enable much more growth opportunity for hybrid layered structures involving MoS_2 with other 2D materials in the future.

dx.doi.org/10.1021/nl4033704 | Nano Lett. 2014, 14, 464–472

Methods. *Deposition of the Seeding Promoter and Growth of MoS_2.* PTAS seeding promoter (50 μM) and CV (crystal violet) (100 μM) were dissolved in water, and a small droplet (2−3 μL) of solution was dropped on a clean 300 nm SiO_2/Si substrate, which was treated by piranha solution to achieve a hydrophilic surface. The solution was spread out to cover the whole surface using the side of a micropipet tip scanning on the surface. Then the drop was dried quickly by a flow of N_2. For the following kinds of seeding promoters, a standard thermal evaporation process (the pressure in the chamber was about 1×10^{-6} Torr) was used to deposit them on the SiO_2/Si substrates: 1 Å F_{16}CuPc, 2 Å PTCDA, 2 Å CuPc, 2 Å DBP, 1 nm NAA, 2 Å spiro-TDP, 1 Å TCTA, 1 Å BCP, 2 Å TPBi, 2 Å spiro-2-NPB, 2 Å $Ir(ppy)_3$, and 5 Å Au. Seeding promoters of 0.7 Å Al_2O_3 and 0.9 Å HfO_2 were deposited on the SiO_2/Si substrate by ALD (atomic layer deposition). After seeding, the substrates were placed facing down on a crucible containing MoO_3 powder. This crucible is put in the middle of a quartz tube reaction chamber, with another sulfur containing crucible upstream in the quartz tube (Figure 1a). Before heating, the whole CVD system was purged with 500 sccm Ar (99.999% purity) for 3 min. Then, 5 sccm Ar was introduced in the system as a carrying gas. The system was heated to 650 °C at a rate of 15 °C/min, and MoS_2 was synthesized at 650 °C for 3 min under the atmospheric pressure. The temperature of sulfur during growth is around 180 °C. The system was finally cooled down to room temperature quickly by opening the furnace and taking out the quartz tube, and 500 sccm Ar flow was used to remove the reactants.

Characterization of the Materials. To characterize the samples, we used AFM (Dimension 3100, Veeco Instruments Inc.) for sample thickness measurement, optical microscopy (Axio Imager, Carl Zeiss) for sample imaging, and PL and Raman (Horiba Jobin-Yvon HR800) for spectroscopy measurements. The excitation wavelength for the PL and Raman measurement is typically 532.5 nm. Some of the spectra were taken using a 632.8 nm wavelength. The laser power on the sample was about 1 mW. A 100× objective was used to focus the laser beam. The spectral parameters were obtained by fitting the peaks using Lorentzian/Gaussian mixed functions. The PL and Raman spectra in comparison are normalized by the A_{1g} Raman mode intensities.

Growth of the Hybrid Structures. For the preparation of MoS_2/Au hybrid structures, 100 nm Au was first deposited on a SiO_2/Si substrate by thermal evaporation. For MoS_2/h-BN and MoS_2/graphene (graphite) growth, mechanically exfoliated h-BN and graphene (graphite) were first transferred to the SiO_2/Si substrate. Then, 1 Å F_{16}CuPc was deposited on these substrates by thermal evaporation. The substrate with the F_{16}CuPc seeding promoter was used to grow MoS_2 monolayers routinely, and this allowed us to prepare the MoS_2/Au, MoS_2/h-BN, and MoS_2/graphene (graphite) hybrid structures directly.

■ ASSOCIATED CONTENT

Supporting Information

CVD setup for the promoter assisted MoS_2 growth; the characterization of the background; mapping images of the other spectral parameters of a typical MoS_2 flake; the MoS_2 growth result on the promoter substrate; growth results for the inorganic particles as seeding promoters; the characterization of the quality of MoS_2 grown by different kinds of seeding promoters; the spectral parameters for the Raman modes and PL peak of MoS_2 by different kinds of seeding promoters; the large-area, continuous, uniform, and high-quality MoS_2 by using 1 Å F_{16}CuPc as seeding promoter; the Raman spectra characterization of the existence of F_{16}CuPc after the growth condition; the growth results of MoS_2 on Au, h-BN, and graphene without using any seeding promoters. This material is available free of charge via the Internet at http://pubs.acs.org.

■ AUTHOR INFORMATION

Corresponding Authors

*Tel: +1-617-324-4068. E-mail: jingkong@mit.edu.
*Tel. and fax: +886-3-5715131, ext 33880. E-mail: yhlee.mse@mx.nthu.edu.tw.

Notes

The authors declare no competing financial interest.

■ ACKNOWLEDGMENTS

This work is partially supported by the National Science Foundation under award number NSF DMR 0845358 and NSF/DMR 1004147. We thank the National Science Council of the Republic of China (NSC102-2633-M-007-002) for partial support of this research.

■ REFERENCES

(1) Geim, A. K.; Novoselov, K. S. *Nat. Mater.* **2007**, *6*, 183−191.
(2) Radisavljevic, B.; Radenovic, A.; Brivio, J.; Giacometti, V.; Kis, A. *Nat. Nanotechnol.* **2011**, *6*, 147−150.
(3) Dean, C. R.; Young, A. F.; Meric, I.; Lee, C.; Wang, L.; Sorgenfrei, S.; Watanabe, K.; Taniguchi, T.; Kim, P.; Shepard, K. L.; Hone, J. *Nat. Nanotechnol.* **2010**, *5*, 722−726.
(4) Wang, H.; Nezich, D.; Kong, J.; Palacios, T. *IEEE Electron Device Lett.* **2009**, *30*, 547−549.
(5) Wang, Q. H.; Kalantar-Zadeh, K.; Kis, A.; Coleman, J. N.; Strano, M. S. *Nat. Nanotechnol.* **2012**, *7*, 699−712.
(6) Wang, H.; Hsu, A.; Wu, J.; Kong, J.; Palacios, T. *IEEE Electron Device Lett.* **2010**, *31*, 906−908.
(7) Wang, H.; Taychatanapat, T.; Hsu, A.; Watanabe, K.; Taniguchi, T.; Jarillo-Herrero, P.; Palacios, T. *IEEE Electron Device Lett.* **2011**, *32*, 1209−1211.
(8) Wang, H.; Yu, L.; Lee, Y.-H.; Shi, Y.; Hsu, A.; Chin, M. L.; Li, L.-J.; Dubey, M.; Kong, J.; Palacios, T. *Nano Lett.* **2012**, *12*, 4674−4680.
(9) Hsu, A.; Wang, H.; Shin, Y. C.; Mailly, B.; Zhang, X.; Yu, L.; Shi, Y.; Lee, Y. H.; Dubey, M.; Kim, K. K.; Kong, J.; Palacios, T. *Proc. IEEE* **2013**, *101*, 1638−1652.
(10) Li, X.; Cai, W.; An, J.; Kim, S.; Nah, J.; Yang, D.; Piner, R.; Velamakanni, A.; Jung, I.; Tutuc, E.; Banerjee, S. K.; Colombo, L.; Ruoff, R. S. *Science* **2009**, *324*, 1312−1314.
(11) Reina, A.; Jia, X.; Ho, J.; Nezich, D.; Son, H.; Bulovic, V.; Dresselhaus, M. S.; Kong, J. *Nano Lett.* **2009**, *9*, 30−35.
(12) Song, L.; Ci, L.; Lu, H.; Sorokin, P. B.; Jin, C.; Ni, J.; Kvashnin, A. G.; Kvashnin, D. G.; Lou, J.; Yakobson, B. I.; Ajayan, P. M. *Nano Lett.* **2010**, *10*, 3209−3215.
(13) Shi, Y.; Hamsen, C.; Jia, X.; Kim, K. K.; Reina, A.; Hofmann, M.; Hsu, A. L.; Zhang, K.; Li, H.; Juang, Z.-Y.; Dresselhaus, M. S.; Li, L.-J.; Kong, J. *Nano Lett.* **2010**, *10*, 4134−4139.
(14) Kim, K. K.; Hsu, A.; Jia, X.; Kim, S. M.; Shi, Y.; Hofmann, M.; Nezich, D.; Rodriguez-Nieva, J. F.; Dresselhaus, M.; Palacios, T.; Kong, J. *Nano Lett.* **2012**, *12*, 161−166.
(15) Lee, Y.-H.; Zhang, X.-Q.; Zhang, W.; Chang, M.-T.; Lin, C.-T.; Chang, K.-D.; Yu, Y.-C.; Wang, J. T.-W.; Chang, C.-S.; Li, L.-J.; Lin, T.-W. *Adv. Mater.* **2012**, *24*, 2320−2325.
(16) Zhan, Y.; Liu, Z.; Najmaei, S.; Ajayan, P. M.; Lou, J. *Small* **2012**, *8*, 966−971.

(17) Liu, K.-K.; Zhang, W.; Lee, Y.-H.; Lin, Y.-C.; Chang, M.-T.; Su, C.-Y.; Chang, C.-S.; Li, H.; Shi, Y.; Zhang, H.; Lai, C.-S.; Li, L.-J. *Nano Lett.* **2012**, *12*, 1538−1544.
(18) Shi, Y.; Zhou, W.; Lu, A.-Y.; Fang, W.; Lee, Y.-H.; Hsu, A. L.; Kim, S. M.; Kim, K. K.; Yang, H. Y.; Li, L.-J.; Idrobo, J.-C.; Kong, J. *Nano Lett.* **2012**, *12*, 2784−2791.
(19) Lee, Y.-H.; Yu, L.; Wang, H.; Fang, W.; Ling, X.; Shi, Y.; Lin, C.-T.; Huang, J.-K.; Chang, M.-T.; Chang, C.-S.; Dresselhaus, M.; Palacios, T.; Li, L.-J.; Kong, J. *Nano Lett.* **2013**, *13*, 1852−1857.
(20) Ji, Q.; Zhang, Y.; Gao, T.; Zhang, Y.; Ma, D.; Liu, M.; Chen, Y.; Qiao, X.; Tan, P.-H.; Kan, M.; Feng, J.; Sun, Q.; Liu, Z.-F. *Nano Lett.* **2013**, *13*, 3870−3877.
(21) Van der Zande, A. M.; Huang, P. Y.; Chenet, D. A.; Berkelbach, T. C.; You, Y.; Lee, G.-H.; Heinz, T. F.; Reichman, D. R.; Muller, D. A.; Hone, J. C. *Nat. Mater.* **2013**, *12*, 554−561.
(22) Najmaei, S.; Liu, Z.; Zhou, W.; Zou, X.; Shi, G.; Lei, S.; Yakobson, B. I.; Idrobo, J.-C.; Ajayan, P. M.; Lou, J. *Nat. Mater.* **2013**, *12*, 754−759.
(23) Wang, X.; Feng, H.; Wu, Y.; Jiao, L. *J. Am. Chem. Soc.* **2013**, *135*, 5304−5307.
(24) Yu, Y.; Li, C.; Liu, Y.; Su, L.; Zhang, Y.; Cao, L. *Sci. Rep.* **2013**, *3*, 1866.
(25) Wu, S.; Huang, C.; Aivazian, G.; Ross, J. S.; Cobden, D. H.; Xu, X. *ACS Nano* **2013**, *7*, 2768−2772.
(26) Weber, T.; Muijsers, J. C.; Van Wolput, J. H. M. C.; Verhagen, C. P. J.; Niemantsverdriet, J. W. *J. Phys. Chem.* **1996**, *100*, 14144−14150.
(27) Sup Choi, M.; Lee, G.-H.; Yu, Y.-J.; Lee, D.-Y.; Hwan Lee, S.; Kim, P.; Hone, J.; Jong Yoo, W. *Nat. Commun.* **2013**, *4*, 1624.
(28) Novoselov, K. S.; Neto, A. H. C. *Phys. Scr.* **2012**, *2012*, 014006.
(29) Yu, W. J.; Li, Z.; Zhou, H.; Chen, Y.; Wang, Y.; Huang, Y.; Duan, X. *Nat. Mater.* **2013**, *12*, 246−252.
(30) Splendiani, A.; Sun, L.; Zhang, Y.; Li, T.; Kim, J.; Chim, C.-Y.; Galli, G.; Wang, F. *Nano Lett.* **2010**, *10*, 1271−1275.
(31) Lee, C.; Yan, H.; Brus, L. E.; Heinz, T. F.; Hone, J.; Ryu, S. *ACS Nano* **2010**, *4*, 2695−2700.
(32) Molina-Sánchez, A.; Wirtz, L. *Phys. Rev. B* **2011**, *84*, 155413.
(33) Aizenberg, J.; Black, A. J.; Whitesides, G. M. *Nature* **1999**, *398*, 495−498.
(34) Wolde, P. R.; ten Frenkel, D. *Science* **1997**, *277*, 1975−1978.
(35) Yu, Q.; Jauregui, L. A.; Wu, W.; Colby, R.; Tian, J.; Su, Z.; Cao, H.; Liu, Z.; Pandey, D.; Wei, D.; Chung, T. F.; Peng, P.; Guisinger, N. P.; Stach, E. A.; Bao, J.; Pei, S.-S.; Chen, Y. P. *Nat. Mater.* **2011**, *10*, 443−449.
(36) http://en.wikipedia.org/wiki/Nucleation.
(37) Fletcher, N. H. *J. Chem. Phys.* **1958**, *29*, 572−576.
(38) Turnbull, D. *J. Chem. Phys.* **1950**, *18*, 198−203.
(39) De Oteyza, D. G.; Barrena, E.; Ossó, J. O.; Sellner, S.; Dosch, H. *J. Am. Chem. Soc.* **2006**, *128*, 15052−15053.
(40) Mouri, S.; Miyauchi, Y.; Matsuda, K. *Nano Lett.* **2013**, *13*, 5944−5948.
(41) Kośmider, K.; Fernández-Rossier, J. *Phys. Rev. B* **2013**, *87*, 075451.
(42) Xiang, Q.; Yu, J.; Jaroniec, M. *J. Am. Chem. Soc.* **2012**, *134*, 6575−6578.
(43) Bernardi, M.; Palummo, M.; Grossman, J. C. *Nano Lett.* **2013**, *13*, 3664−3670.
(44) http://www.lumtec.com.tw/about.asp.
(45) http://www.sigmaaldrich.com/catalog/product/fluka/53882?lang=en&region=US.